Title

Reduced bandwidth Compton photons from a laser-plasma accelerator using tailored plasma channels

Journal

Physics of Plasmas, 28(12)

ISSN

1070-664X

Authors

Grote, DP
Friedman, A
Geddes, CGR
et al.

Publication Date

2021-12-01

DOI

10.1063/5.0073622

Peer reviewed

Reduced bandwidth Compton photons from a laser-plasma accelerator using tailored plasma channels

D. P. Grote[1†], A. Friedman[1], C. G. R. Geddes[2], R. Lehe[2], C. Benedetti[2], T. M. Ostermayr[2], H-E Tsai[2], J.-L. Vay[2], C. B. Schroeder[2], E. Esarey[2]
[1]*Lawrence Livermore National Security, Livermore, CA 94550*
[2]*Lawrence Berkeley National Laboratory, Berkeley, California 94720, USA*

Abstract

It has been demonstrated experimentally that laser plasma accelerators can produce multi-100 MeV electron bunches with a few percent energy spread, and from these electrons multi-MeV quasi-monoenergetic photons have been demonstrated based on Compton up-scattering from a counter-propagating laser. This offers the potential of a high quality, narrow bandwidth, compact, photon source with broad application. The bandwidth of the resulting photons depends directly on the distribution of the electron bunch and is limited in particular by the bunch divergence (i.e., the spread in transverse velocity angle). At the same time, the ability to decelerate electrons after scattering is important to source deployment. We describe a series of plasma structures that expand and then collimate the electron bunch, reducing its divergence and thus reducing the bandwidth of the scattered photons while enabling both high performance scattering and deceleration. These plasma structures are demonstrated in simulations of the accelerator system, showing the potential to reach few-percent photon spread which is important for applications using Nuclear Resonance Fluorescence.

Introduction

Narrow bandwidth photon sources could greatly improve the efficiency and sensitivity of systems that use high energy photons for detection, characterization, and screening of special nuclear materials [1,2, 13-16]. Current photon sources use conventional accelerators to produce electron beams and generate photons via Bremsstrahlung, resulting in radiation with a broad energy spread. Compton (or Thomson) scattering has the potential to produce narrow energy spreads, but requires a much higher electron energy, and, hence, to date has been restricted to large research facilities [3-6]. In such a source, high-energy photons are generated by backscattering visible to infrared photons off the accelerated electrons, upshifting the photon energy – GeV electrons are required to produce photons of few 10s of MeV.

In multiple facilities, laser plasma accelerators [7] (LPAs) have been developed allowing GeV-class electrons with small spreads in energy and in cm-scale distances [8-11]. The radiation pressure of a relativistically intense laser pulse pushes aside the plasma electrons, which are pulled back by the ions (which are effectively stationary for typical laser parameters), creating a "bubble" of positive charge following the laser and a "wakefield" that can have GeV/cm level accelerating (and focusing) gradients [7]. Relativistic intensity is characterized by a normalized peak laser vector potential $a_0 \geq 1$, where $a_0 = eA_{\max}/m_e c^2 = (2e^2\lambda^2 I/\pi m_e^2 c^5)^{1/2}$, and $A_{\max}$ is the peak laser vector potential, I the peak laser intensity, λ the laser wavelength, e the electron charge, m_e the electron mass, and c the speed of light. This corresponds to an intensity $\geq 10^{18}$ W/cm^2 near 1 μm laser wavelength. For example, Leemans *et. al.* [8] have shown electron beams

† Corresponding author. Email: grote1@llnl.gov

with energy in the range of 500 MeV to 1 GeV, with percent level energy spreads. These beams were obtained by using plasma channels, realized with a capillary discharge to guide the laser, allowing a multi-centimeter acceleration length. These GeV, low-energy-spread beams provide the possibility of producing a compact source of low-energy-spread, quasi-monoenergetic, photon pulses by means of Compton scattering. Hence, an LPA source provides the possibility of realizing a compact, mobile source with a high degree of energy flexibility.

In the system of interest, a drive laser accelerates an electron bunch (formed by one of several means of injection [7]) via the laser-plasma wakefield acceleration process. In the region where the electrons reach their peak energy, they interact with a counter-propagating scattering laser to produce the high-energy photons by means of electron-photon Thomson scattering. Photons are scattered at all angles, but because of the high velocity of the electrons, half of the scattered photons are backscattered within a cone angle given by $\theta \sim 1/\gamma_e$, where γ_e is the relativistic gamma factor of the electrons. The highest energy photons, with a frequency of $4\gamma_e^2\omega_L$, where ω_L is the scattering laser frequency, are purely backscattered, creating a quasi-mono-energetic forward-going photon beam. Furthermore, rather than dumping the accelerated electrons after scattering, which would require a large shielding mass, the laser-wakefield acceleration process can be used in reverse, letting the electrons reach the forward side of the plasma "bubble" formed by the drive laser (or by a secondary laser), where the wakefield decelerates the electrons [1, 12]. To accomplish this, a structure is needed in which no significant additional electrons will be trapped, and through which the scatter laser can propagate without disturbance to reach the scattering point.

An LPA system is anticipated to be able to provide the photon rate required for rapid scanning, which is of order 10^{10} to 10^{12} photons/second [2,13-16], by producing 10^6 to 10^8 photons per pulse and operating at pulse rates of 1 kHz to a few 10s of kHz. The per-pulse photon number has been demonstrated in LPA-based Compton scattering experiments [17-20,44-46], and compact laser drivers at kHz rates are being developed [21]. To date, photon energy spreads have been in the tens of percent range, which begins to allow for radiography and photofission [2,13-16]. While this energy spread level would already enable strong improvement over conventional sources, increased effectiveness would be possible with reduction of energy spread below 10%. This would enhance ability to stimulate the desired signatures while avoiding photoneutron production, which is present for energies above 9 MeV [2]. Furthermore, many applications motivate the use of highly specific Nuclear Resonance Fluorescence (NRF) [2]. Hence, an important challenge for the ongoing development of such sources is to achieve a sufficiently narrow bandwidth at or below the few percent level needed to enable NRF. For such signatures, photon energies of 1.7 MeV (for Uranium) to above 7 MeV (for energetic materials) are of interest. The major driver of the energy spread of the high energy photons is the quality of the accelerated electron bunch. While plasma accelerators have produced electron energy spreads that could by itself enable a 2% photon energy spread [8,22,23,41], the divergence of the electron bunch, however, also has a direct impact on the energy spread of the scattered photons and to date has been at a level that would prevent reaching such energy spreads. Reducing divergence by refocusing or other methods is hence an important aspect of such sources. Here, divergence is defined as the spread in velocity angles. For example, the rms divergence can be written as $\sigma_{\theta,\mathrm{rms}}{}^2 = \langle(\tan^{-1} {}^{v_\perp}/_{v_z})^2\rangle$, averaging over the particles and where $v_\perp$ and v_z are the transverse and longitudinal velocities of the particles. While it is well known that refocusing can be accomplished using magnetic electron beam optics, such systems are bulky (negating much of

the compactness that motivates an LPA based source) and are often incompatible with deceleration due to the bunch stretching induced by the optics.

The bandwidth of the scattered photons depends on the longitudinal and transverse velocity spreads of the electron beam, the laser amplitude, and multiple scattering with the scattering laser, with these effects adding in quadrature. Here we focus on the transverse spread of the electrons, which is a key limiting factor as shown by previous simulation studies [24]. Photons scattered by electrons that have a significant transverse velocity (i.e., $\theta > 1/\gamma_e$) will produce photons scattered towards the target with energy less than that obtained from scattering off well-collimated electrons, leading to energy spread of the photon pulse. The contribution of this effect to the photon bandwidth scales as the square of the electron divergence angle [24].

In this paper we show that photon source bandwidths at the few percent level can be achieved by reducing the divergence of the electron bunch after acceleration in a structure consistent with high performance deceleration. The required manipulation of the electron bunch can be accomplished by modifying the plasma structure in the region after acceleration, before and during the region where scattering occurs. This allows for acceleration, beam manipulation, MeV photon production (scattering), and electron beam deceleration all within cm-scale distances. We describe the design process for such plasma structures and provide a specific case designed to produce ~7 MeV photons, an energy in the range of multiple applications.

The paper is organized as follows. The following section, "Plasma Channel," includes results from simulations of the system with the plasma structure, its effect on the electron bunch, and the resulting photon distribution. In the subsequent section, "Deceleration", we discuss issues related to the deceleration section that affect both the electron bunch and scattering laser. The final section is the conclusions.

Plasma channel

With control of the gas density, and therefore of the plasma density, it is possible to generate plasma structures that can compactly tailor the properties of the electron bunch to reduce the scattered photon bandwidth. These rely on the fact that the wakefield focusing force is comparable to its accelerating force, and is many orders of magnitude greater than that obtained with conventional magnets. These forces keep the electron bunch focused to diameters less than a micron within the accelerator [25], but correspondingly even low emittance bunches will have mrad level divergence which degrades photon source bandwidth. Reduction of the divergence of the bunch can be achieved by adding a vacuum region and a plasma-based focusing element after the accelerating stage. The vacuum region leads to expansive cooling that reduces the local transverse velocity spread of the beam. The transverse size of the beam can indeed be allowed to expand by an order of magnitude without significantly affecting the scattering interaction, since the scatter laser focal spot is typically at the 10 μm scale to allow sufficient focal depth for high yield scattering [24]. The beam transverse expansion leads to a direct reduction in the beam local transverse velocity spread by the same order of magnitude. After the beam expands, a further plasma structure can then be used as the focusing element to collimate the electrons, the rotation in phase-space converting the reduced local transverse velocity spread into a reduced divergence. The collimated bunch then interacts with the scattering laser. After the scattering, the drive laser enters a final plasma structure, creating a new plasma "bubble" whose wakefeld carries out the deceleration process.

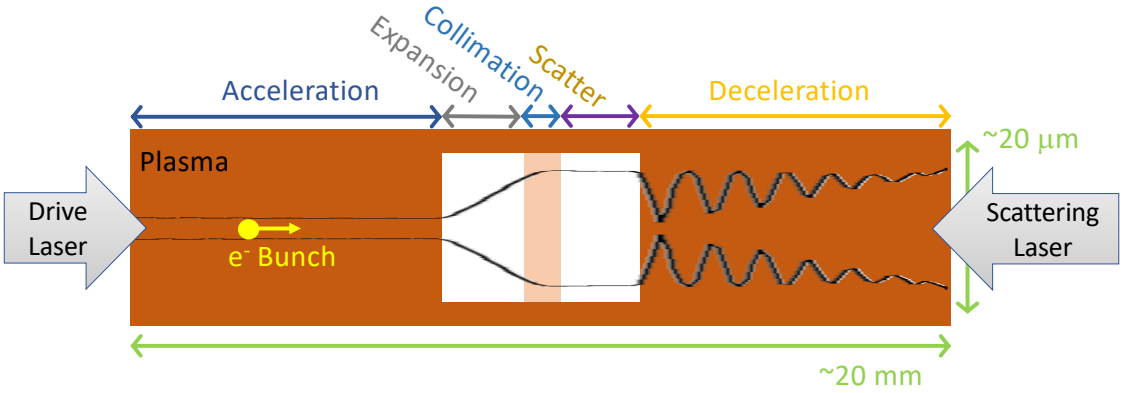

Figure 1. Layout of the plasma structure. The black curves denote the electron bunch envelope. Note that the envelope, of order ~1 μm after expansion, is plotted at an enlarged scale to be visible in the 20 μm vacuum region diameter.

The overall plasma is structured both transversely and longitudinally to accomplish acceleration, tailoring of divergence, scattering, and deceleration as shown in Figure 1. Transversely, it has a lower density plasma on axis surrounded by a higher density plasma "cladding" that acts to continually focus the drive laser throughout the acceleration, scatter, and deceleration processes [26,27], even in the vacuum regions. The plasma around the axis has a parabolic transverse density profile, providing additional focusing in the higher density regions. Initially, the plasma "bubble" that forms in the wake of the laser accelerates the electrons and provides a transverse force that keeps the electrons focused [28]. At the point where the electrons reach their highest energy, before they dephase from the accelerating field, the plasma density on axis is reduced nearly to zero, causing the "bubble" fields to become tenuous; this ends the acceleration and the transverse focusing, and allows the electrons to freely expand. The length of this plasma void is tuned so that the electrons expand to the desired degree. Then, a plasma with low density is introduced, setting up a plasma lens that stops the expansion of the electrons and collimates the beam [42]. The plasma lens is created by the wake of the drive laser in the low-density plasma. The lens is short, and no significant (de)acceleration occurs. After this collimation, the plasma density is again reduced to allow the collimated electrons to free stream and interact with the scattering laser (Compton scattering). In the final section, the plasma density on axis is increased to a value comparable to the one in the accelerating stage, allowing the plasma "bubble" to re-form as the drive laser enters it, providing for deceleration of the electrons. Tailoring of this section's density to prevent undesired trapping or modulation of the scatter laser is addressed in the following section. Note that the accelerating section was designed to avoid strong laser depletion and to keep the laser focused so that there is sufficient laser intensity to re-form the plasma bubble for deceleration. This is a different optimization criterion from an acceleration-only system which would aim at strongly depleting the laser in the acceleration stage for efficiency. The details of this deceleration are described in a later section of this paper.

An accelerator designed to produce nearly 600 MeV electrons is used as an example, producing 7 MeV photons after the interaction with a scattering laser with a wavelength λ_{sc} = 0.8 μm. The design was generated by performing a series of simulation scans, beginning from theoretical or experimental baselines, and with each scan sequentially optimizing one aspect of the design. The overall system design was set by balancing application requirements and physics

constraints. The drive laser is a bi-Gaussian pulse with a_0 = 2.5, wavelength λ = 0.8 μm (the corresponding peak intensity is 1.34×10^{19} W/cm^2), rms pulse length 10 μm, and focal waist radius of 10 μm (the laser is focused at the plasma channel entrance). The chosen laser amplitude is a balance of setting the power high enough to trigger injection of an electron bunch [40], but low enough to avoid complete laser depletion. The accelerator section is an H^+ plasma with a density of 1.5×10^{24} m^{-3} along the center of the guiding channel, parabolically increasing out to a radius of 20 μm, greater than the laser waist radius, up to a density of 6.0×10^{24} m^{-3}. The density was selected based on past simulations [24], theoretical scalings [7], and experiments [8]. The parabolic channel parameters were based on nonlinear corrections [29,30] to the channel guiding formulas [7] to maintain the laser focus at this amplitude. Beyond 20 μm radius, the density is fixed at 6.0×10^{24} m^{-3} providing the "cladding".

The simulations were carried out using the FBPIC code [31,32], which uses a spectral-cylindrical representation of the system, with azimuthal Fourier decomposition of the electromagnetic fields. Two azimuthal modes were used, and the simulation operated in a Lorentz boosted frame [43] with a gamma boost of 10. Various sets of numerical parameters were used, with values typically around 200 radial and 3600 longitudinal grid cells for a domain that is 100 μm in radius and 72 μm long. Of order 20 million particles were used to model the background plasma, and 30,000 to model the electron bunch. The simulation results of the final design, showing the electron bunch profile and energy, can be seen in Figure 2 and Figure 3.

While the design was set up to be consistent with a realizable experiment with a self-injected electron bunch, instead of relying on self-injection, a bunch representative of past injection experiments is preloaded in the simulation, reducing the complexity of the simulations. The phase of the bunch relative to the drive laser is adjusted to give the desired peak energy. The optimal value was found when the bunch is 16 μm (or ~3.7 skin depths) behind the laser peak. A series of simulations was carried out to determine the properties of the pre-loaded electron bunch. The timing of the electron bunch with respect to the laser pulse was adjusted to control the initial phase of the bunch within the acceleration bubble, which sets the peak energy obtained. A bunch charge of 36 pC and an rms bunch length of 0.3 μm (with a Gaussian distribution) was determined to have an optimal value of the beam loading, counteracting the nonuniform longitudinal acceleration field, again determined by a scan of simulations. This amount of charge is consistent with what has been obtained in experiments [33,34]. This reduces the energy spread of the bunch leading to an improvement in the quality of the scattered photons and the deceleration. Note that the degree of beam loading depends on the bunch line-charge density, so that the optimal charge will be dependent on the bunch length. The additional parameters of the bunch include an rms radius of 0.25 μm, a transverse normalized emittance of 0.1 μm-rad, an initial gamma of 100 with an rms spread $\delta\gamma = 1$. In a system with injection, such as down-ramp or ionization injection, there will be equivalent controls of the phase and charge by adjusting the injection scheme.

The peak energy of 560 MeV with 2% energy spread and 0.8 mrad rms divergence is reached shortly after 8 mm of acceleration, as can be seen in Figure 3. These parameters are consistent with past experiments [1,22]. An estimate of the photon energy spread is given by [24]:

$$BW > \sqrt{\frac{\gamma_e^4 \sigma_{\theta,FWHM}^4}{16} + \frac{4\sigma_{(\gamma_e),FWHM}^2}{\gamma_e^2} + \frac{a_0^4}{2}}. \quad (1)$$

Here $\sigma_{\theta,FWHM}$ is the transverse divergence and $\sigma_{(\gamma_e),FWHM}$ is the energy spread. With a_0 = 0.25 for the scattering laser, the bandwidth is 100%, dominated by the contribution of the divergence. If all the divergence could be removed, this would give a bandwidth of 4%. The drive laser retains ~60% of its energy for the deceleration stage.

At the point where the bunch reaches peak energy, the cylindrical vacuum region is inserted, allowing the free expansion of the beam. To determine the length of the vacuum region, a scan of simulations varying this length was conducted. For this design, a length of 1 mm was found to give the maximum reduction of divergence achievable after collimation. Further expansion did not lead to further decrease of the divergence after collimation, the remaining amount being due to the longitudinal velocity spread and the coupling between longitudinal and transverse velocities that occurs in the plasma lens collimator. To collimate the electron beam, a low-density plasma region with uniform longitudinal and parabolic transverse density profiles was used. The length of the lens was 0.5 mm, and the plasma density in the lens was ~7% of the nominal channel density. Multiple simulation scans were done to optimize the lens performance. In this moderate density plasma, the laser driven wake acts as a plasma lens, providing enough of a focusing force on the beam to stop the expansion. In this example, the beam radius expands from 0.1 μm to 0.8 μm, as can be seen in Figure 2. A commensurate factor of 8 reduction of the divergence was obtained, from 0.8 mrad, which is typical of experiments at this energy, to 0.1 mrad. With this reduced amount of divergence, the bandwidth estimate above is 5%. Throughout the bunch expansion and scattering region, the "cladding" plasma density remains constant, acting as a hollow plasma channel [35] which prevents the laser from expanding so that its intensity is preserved for the subsequent deceleration region.

A second cylindrical vacuum region is placed after the electron beam collimation, forming the scattering region. Its length of 1 mm is approximately the Compton scattering length for the 1 Joule, 2 ps, 0.8 μm wavelength, a_0 = 0.344, scattering laser pulse that is matched to the plasma channel [24]. With this length, there is likely only one scattering event, or fewer, per electron. A longer length would allow multiple scatters, which would lead to added energy spread in the high-energy photons because of the energy loss of the electrons from each scatter. Over this length, there is little transverse expansion of the electron bunch, as can be seen in Figure 2 between the vertical bars, and little change in the bunch energy, as shown in Figure 3. For the purpose of the Compton scattering in the simulations, the scattering laser is applied as a fixed analytic photon density with a Gaussian profile and assumed to be collimated in the channel with a radius of 10 μm. The laser is timed so that the peak passes the center of the scattering region at the same time as the center of the electron bunch. As is shown below, using a prescribed profile is a reasonable approximation since the scattering laser can be propagated upstream through the plasma with little perturbation.

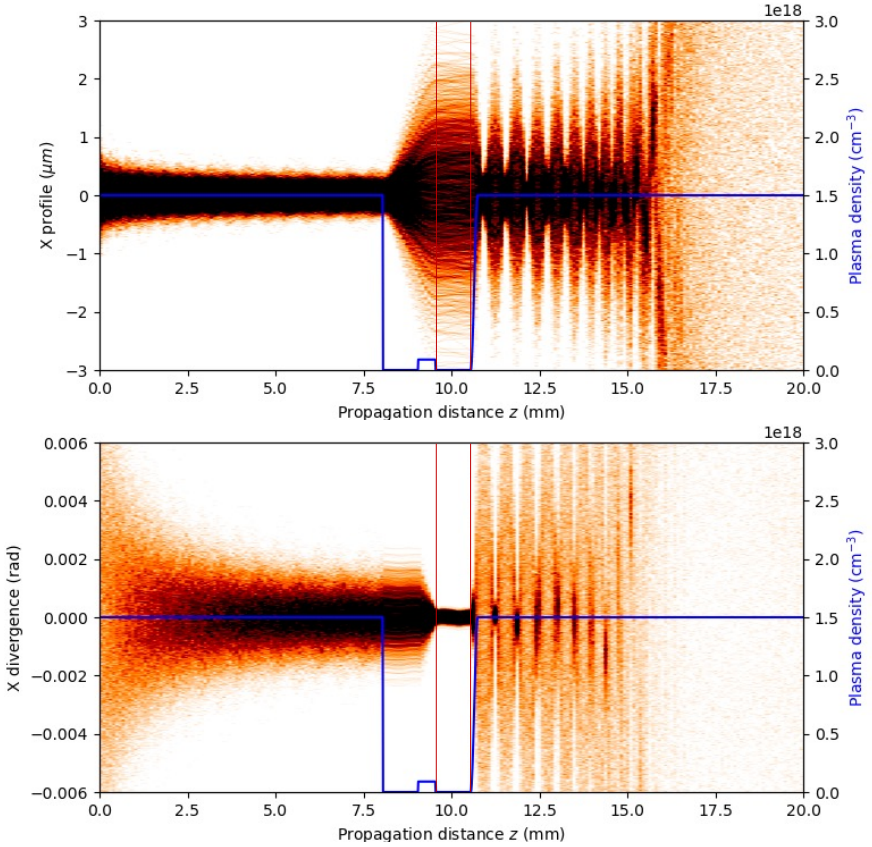

Figure 2. The electron bunch transverse (X) profile (upper plot) and divergence (lower plot) as a function of the propagation distance. The images consist of many snapshots of the bunch as it moves through the channel, with darker color at higher density. The plots also show the plasma density on axis (represented by the blue line). The transverse expansion can be seen between 8.05 and 9.55 mm and the scattering region (with collimated bunch) between 9.55 and 10.55 mm (between the vertical bars). In the deceleration region after 10.55 mm, the bunch becomes strongly mismatched, though it is still confined within the deceleration bubble. After ~17 mm, the deceleration process is complete and the bunch is no longer confined.

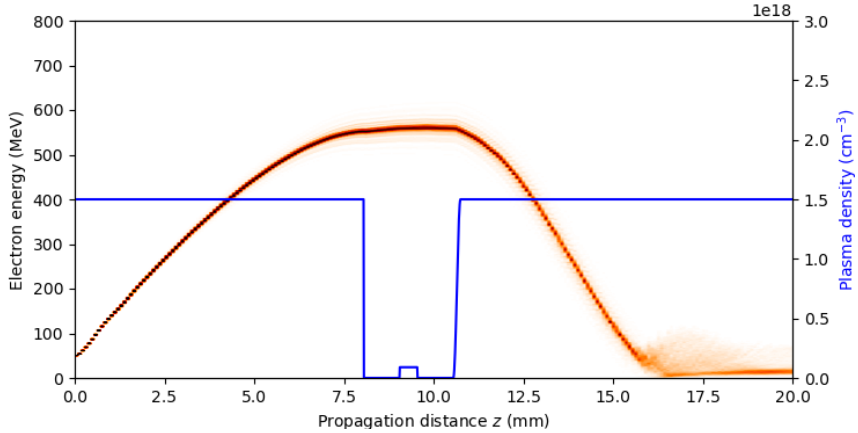

Figure 3. Electron bunch energy as a function of the propagation distance. The image consists of many snapshots of the bunch as it moves through the channel, with darker color at higher density. This also shows the background plasma density on axis (represented by the blue line). Note that this includes only the externally injected electrons. See Figure 5 for consideration of plasma trapped electrons.

The photon distributions, generated with and without the transverse expansion and collimation of the electron bunch, can be seen in Figure 4. In the case without the manipulation, the scattering is done in the region after the peak energy is reached, at 8 mm. The divergence reduction resulted in a significant improvement in the quality of the photon distribution. The FWHM energy spread (as a fraction of the peak photon energy) of the backscattered photons ($\gamma\theta = 0$) is smaller, 5% versus 35%. Also, the photons are focused into a significantly narrower cone angle, putting more photons on the target, with a cone angle, $\gamma\theta$, of ~0.15, versus ~1. In the improved case, there are ~10^7 photons within the FWHM around the peak photon energy, giving ~0.03 photons per electron. The significant improvement in the photon bandwidth, a factor of ~7, is consistent with, though somewhat smaller than, the estimate given above. This example case was not intended to be optimal and it only provides an indication of the improvement that might be obtained. Because of the strong dependence of the bunch properties on the technique used for bunch injection, a true optimization would need to include those details in the model. It is expected that some injection techniques, such as two-color ionization injection [37], could produce bunches with lower emittance, allowing further reductions in bandwidth compared to this example case, thus meeting the < 2% bandwidth requirement needed for NRF applications.

In the FBPIC simulations, the particle electrons are scattered with the prescribed Gaussian laser profile using the Klein-Nishina cross section in the electron rest frame. The assumption of single photon scattering is valid since $a_0 \leq 0.3$, where a negligible amount of the backscatter is in harmonics [47]. The electrons lose energy from a scatter, but the laser profile is not attenuated. The scattering events produce photons that are tallied in the post processing. To improve the statistics, the numerical weight of the photons was set much less than the weight of the electrons so that scattered photons can be created from each simulation electron as much as every time step. Though, to produce the correct electron momentum distribution, the probability of electron scattering (as associated energy loss) is treated as if it is scattering from an equally weighted photon.

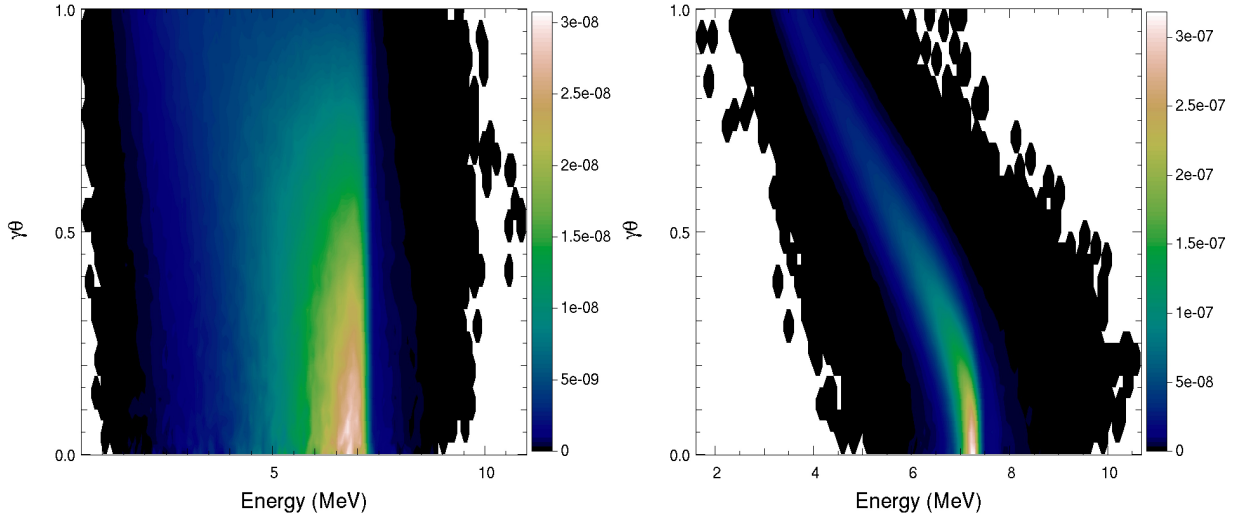

Figure 4. Comparison of the photon distribution, $d^2N/d\omega d\Omega$, without (left) and with (right) the manipulation of the electron bunch.

Deceleration

After the scattering, a further plasma section is used for deceleration, with a density comparable to that in the acceleration section. The driver (or secondary laser) creates a new "bubble" with the associated longitudinal and transverse fields. In the simulations, the drive laser propagated through the system and drove all stages of the process. At the deceleration stage, the electron bunch has de-phased and is in the decelerating phase of the bubble. Because of the bunch expansion in the vacuum region, the bunch is highly mismatched to the transverse fields when it enters this plasma section (as can be seen in the strong envelope oscillations in Figure 2 for $z > 10.5$ mm). However, the bunch remains well confined within the bubble and the mismatch does not appear to degrade the deceleration process. As shown in Figure 6, most of the bunch electrons are decelerated to below 50 MeV. The decelerated energy could potentially be reduced by further tailoring of the plasma profile [36], but since the details of the deceleration depend heavily on the bunch properties, such optimization would require a fully integrated simulation including the bunch injection process which was beyond the scope of this study.

The deceleration section affects the overall system design and can have an indirect effect on the scattering and photon quality because of its effect on the scattering laser, which typically propagates upstream through the deceleration plasma. If the plasma density is constant, the drive laser can trigger the undesired self-injection of background electrons, yielding the formation of secondary electron bunches that are accelerated to an energy of up to a GeV, as shown in the upper panel of Figure 5 for $z > 10$ mm, counter to the desired effect of the deceleration region. The secondary bunches can be reduced by tailoring the plasma density profile in the deceleration section, for example by imposing a linearly increasing ramp in the density. This increases the phase velocity of the plasma bubbles, significantly reducing the generation of secondary bunches. The improved case can be seen in the lower panel of Figure 5. Figure 6 shows the energy distribution of the electrons after deceleration, showing the significant reduction in the high energy electrons with the ramped density. It has been shown that further tuning can eliminate more of the secondary electrons [36], but this will depend on the details of the system and so was not pursued for this test design. The modification of the density profile does not have a significant impact on the deceleration of the primary bunch, though it does delay it, requiring a somewhat longer deceleration section.

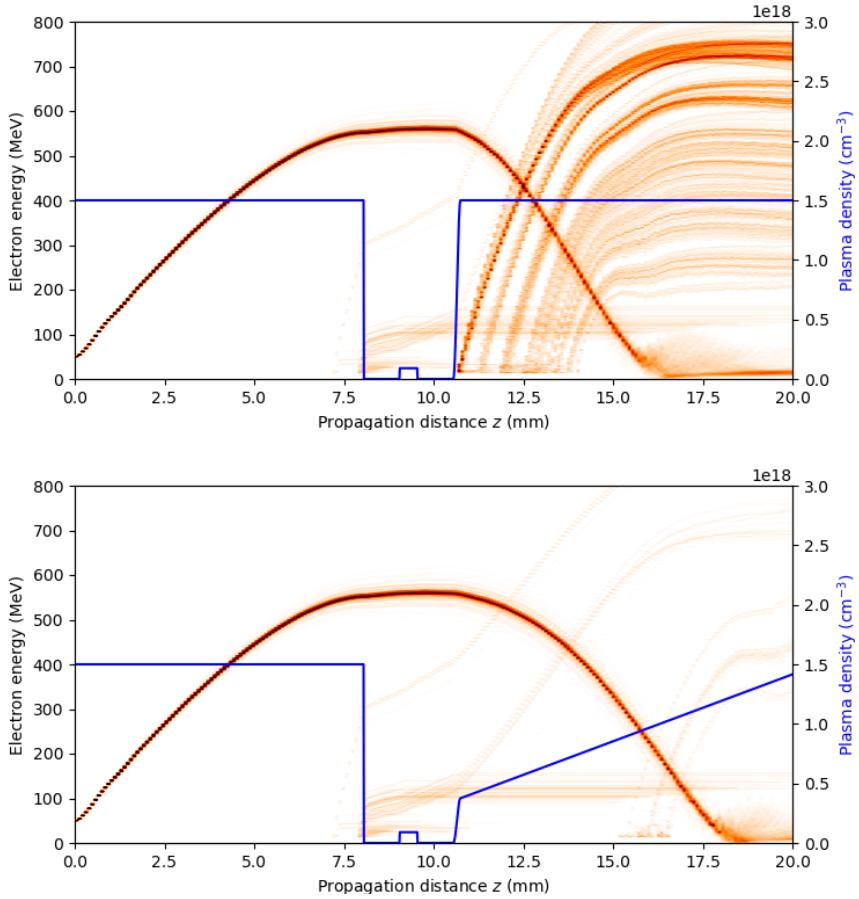

Figure 5. Evolution of the electron energy spectrum, including the preloaded bunch and the secondary electrons from self-injection, for two different density profiles in the decelerating section (represented by a blue line). The images consist of many snapshots of the bunch and accelerated background electrons as they move through the channel, with darker color at higher density. Upper panel: The on-axis density is uniform in the deceleration section, producing the undesirable secondary bunches. Note that this is the same plot as shown in Figure 3 but with the accelerated background electrons included. Lower panel: The on-axis density has a linearly increasing ramp, significantly reducing the formation of the secondary bunches.

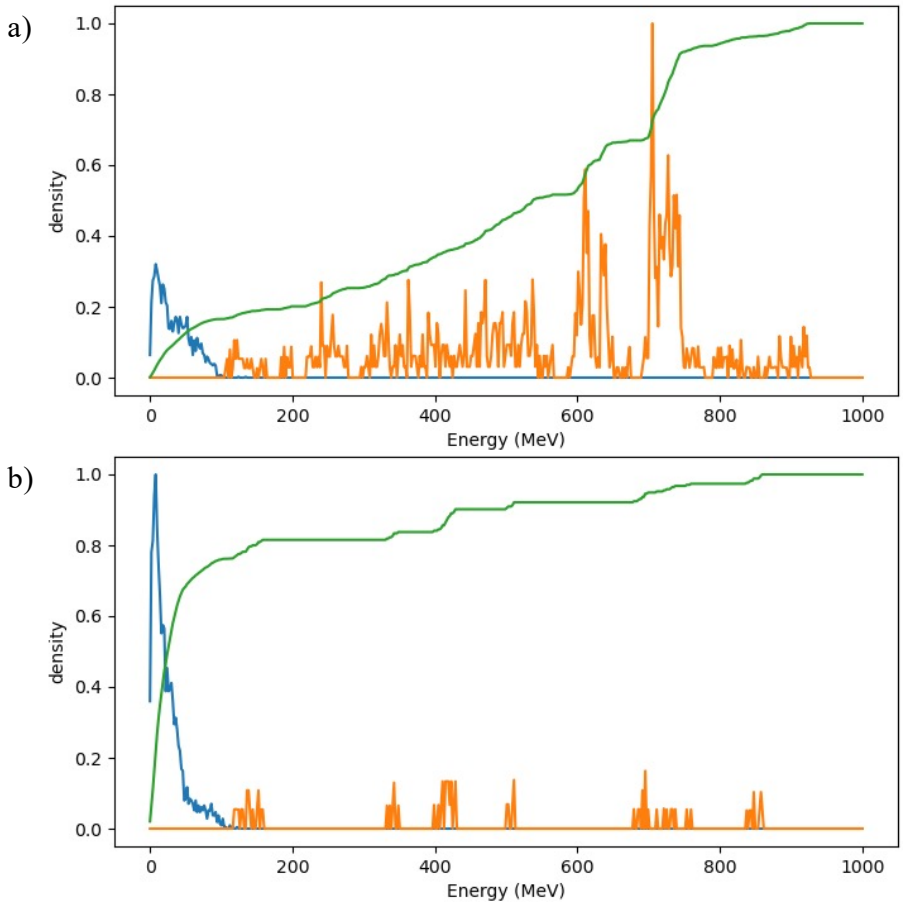

Figure 6. Energy distribution of electrons after deceleration, a) with a uniform density in the deceleration region, at z = 16.5 mm, and b) with a ramped density, at z = 18.5 mm. The plots show the spectral density (particles per MeV) of the bunch (blue) and accelerated background electrons (orange), and the cumulative spectral density (total particles up to the given energy) (green), both normalized.

The ramping of the plasma density offers the additional benefit of improving the behavior of the counter-propagating scattering laser, which must travel through the plasma in the deceleration region. The laser intensity and plasma density create conditions such that the self-modulation instability can grow, degrading the scattering laser pulse [38,39]. The self-modulation instability arises from the feedback between the perturbed plasma density and the focusing and defocusing effects of the perturbed plasma on the laser. The pulse front perturbs the plasma (via the ponderomotive force), producing plasma waves, and this perturbation causes the subsequent part of the laser to focus (in regions where the perturbed plasma density has a local minimum) or defocus (regions where the perturbed density has a local maximum) enhancing the perturbation in the plasma density, further increasing the focusing and defocusing of the laser pulse. This leads to strong laser and plasma density oscillations that can adversely affect both the scattering and deceleration processes. The density ramp sets up a head-to-tail variation of the plasma oscillation wavelength along the pulse that acts to detune the instability, nearly eliminating it. To examine the effect of the instability, simulations were carried out of the scattering laser propagating upstream through the deceleration plasma. The results are shown in

Figure 7, which compares the simulated laser envelopes in the scattering region after propagating through the deceleration plasma (from the right). With a constant density, the laser pulse shows sign of significant self-modulation, but with a density ramp the perturbations are minimal. Since it is more susceptible to instability and therefore more challenging, a flat-topped pulse was used in the simulations. Note that this differs from the Gaussian pulse used for the scattering in the electron bunch simulations, though this should not affect the results since the scattering should be fairly independent of the profile since the laser is not propagated self-consistently in the electron bunch simulations and the bunch does not change significantly during the scattering – it is only the integrated photon density that is important. As with the other simulations, these were done using the FBPIC code, though operating in the lab frame. The cell size in the simulation was 1 μm longitudinally and 0.5 μm radially, with the domain large enough to include the radial extent of the laser and the propagation length.

With an up-ramp in plasma density profile, the simulations indicate that effective deceleration of the main electron bunch can be achieved while mitigating key issues that could otherwise limit such sources. Both acceleration of undesired electrons by the drive laser and modulation of the scattering laser are significantly reduced, showing a path to get to a level consistent with photon source operation.

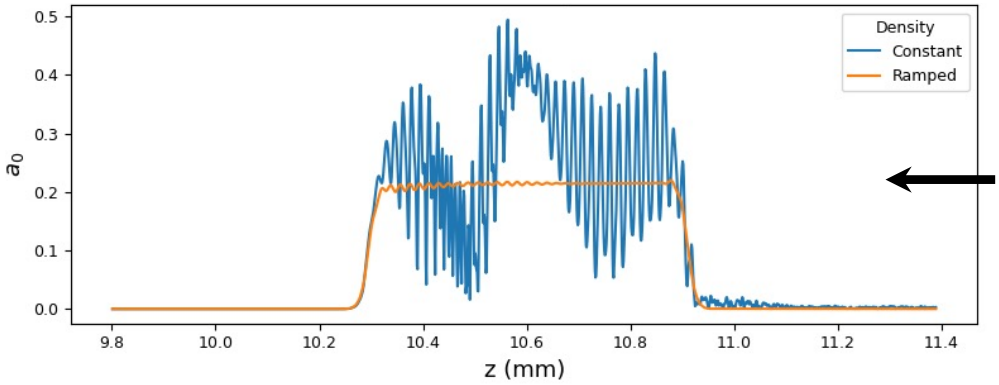

Figure 7. Comparison of the scattering laser envelopes as they enter the scattering region after propagating through the deceleration plasma (propagating from right to left) with and without a density ramp. The density ramp detunes the self-modulation instability, nearly eliminating it.

Conclusion

Laser plasma accelerators are now able to produce high-energy electron bunches with small enough energy spreads that they are attracting interest as compact sources of high energy photon pulses. Development is needed to meet the tight photon bandwidth requirements of several important applications. We have shown a plasma channel designed to manipulate the accelerated electron bunch, reducing its divergence, which in turn reduces the bandwidth of the photons. For the case presented, the bandwidth of the resulting photons was decreased by a factor of 7, pushing it closer to the few percent bandwidth needed for many applications. At the same time, it controls deceleration of the particle bunch after scattering and shows the way toward eliminating secondary accelerated electrons, to enable a compact source footprint without excessive shielding and is consistent with the need for scattering laser propagation through the decelerating section. As the formation of transverse parabolic channels and other plasma structures is well established, it is anticipated that adaptation of existing gas jet and laser control

technology can allow construction of such plasma channel. This work represents a step on the path toward developing a compact high energy, narrow bandwidth, photon source.

Acknowledgements

This work is supported by the U.S. Department of Energy, NNSA DNN R&D and SC HEP under Contract No. DE-AC02-05CH11231 at Lawrence Berkeley National Laboratory and under Contract DE-AC52-07NA27344 at Lawrence Livermore National Laboratory. This research used the Lawrencium computational cluster resource provided by the IT Division at the Lawrence Berkeley National Laboratory (Supported by the Director, Office of Science, Office of Basic Energy Sciences, of the U.S. Department of Energy under Contract No. DE-AC02-05CH11231). We acknowledge Pierre Pelletier for contributions to the FBPIC code that were instrumental to this research.

Data Availability

The data that support the findings of this study are available from the corresponding author upon reasonable request. The data consists of many input files for the FBPIC code for the various input conditions and system designs, multiple Python scripts for the post-processing analysis of the simulation results, and the FBPIC code (which is publicly available).

Author Declarations

The authors have no conflict of interest to disclose.

References

1. C. G. R. Geddes, S. Rykovanov, N. H. Matlis, S. Steinke, J.-L. Vay, E. Esarey, B. Ludewigt, K. Nakamura, B. J. Quiter, C. B. Schroeder, C. Toth, W. P. Leemans, Compact quasi-monoenergetic photon sources from laser-plasma accelerators for nuclear detection and characterization, Nuclear Instruments and Methods in Physics Research B 350, 116 (2015). https://doi.org/10.1016/j.nimb.2015.01.013
2. C. G. R. Geddes, B. Ludewigt, J. Valentine, B. J. Quiter, M.-A. Descalle, G. Warren, M. Kinlaw, S. Thompson, D. Chichester, C. Miller, S. Pozzi, Impact of Monoenergetic Photon Sources on Nonproliferation Applications Final Report. United States: N. p., 2017. https://doi.org/10.2172/1376659
3. H. R. Weller, M. W. Ahmed, H. Gao, W. Tornow, Y. K. Wu, M. Gai, R. Miskimen, Research opportunities at the upgraded HIgS facility, Proc. Part. Nucl. Phys. 62 (2009) 257. https://doi.org/10.1016/j.ppnp.2008.07.001
4. F. Albert, S. G. Anderson, D. J. Gibson, C. A. Hagmann, M. S. Johnson, M. Messerly, V. Semenov, M. Y. Shverdin, B. Rusnak, A. M. Tremaine, F. V. Hartemann, C. W. Siders, D. P. Mcnabb, C. P. J. Barty, Characterization and applications of a tunable, laser-based, MeV-class Compton-scattering gamma-ray source, Phys. Rev. ST-AB, 13 (2010) 070704. https://doi.org/10.1103/PhysRevSTAB.13.070704
5. O. Teşileanu, D. Ursescu, R. Dabu and N. V. Zamfir, Extreme Light Infrastructure – Nuclear Physics, Journal of Physics: Conference Series 420 (2013) 012157. https://doi.org/10.1088/1742-6596/420/1/012157

6. R. Hajima, N. Kikuzawa, N. Nishimori, T. Hayakawa, T. Shizuma, K. Kawase, M. Kando, E. Minehara, H. Toyokawa, H. Ohgaki, Detection of radioactive isotopes by using laser Compton scattered gamma-ray beams,' Nuclear Instruments and Methods in Physics Research A 608, (2009) 557. https://doi.org/10.1016/j.nima.2009.05.063
7. E. Esarey, C. B. Schroeder, and W. P. Leemans, Physics of laser-driven plasma-based electron accelerators, Rev. Mod. Phys. **81**, 1229 (2009). https://doi.org/10.1103/RevModPhys.81.1229
8. W. Leemans, B. Nagler, A. Gonsalves, Cs. Tóth, K. Nakamura, C. G. R. Geddes, E. Esarey, C. B. Schroeder, and S. M. Hooker, GeV electron beams from a centimetre-scale accelerator, Nature Phys **2,** 696–699 (2006). https://doi.org/10.1038/nphys418
9. X. Wang, R. Zgadzaj, N. Fazel, Z. Li, S. A. Yi, X. Zhang, W. Henderson, Y.-Y. Chang, R. Korzekwa, H.-E. Tsai, C.-H. Pai, H. Quevedo, G. Dyer, E. Gaul, M. Martinez, A. C. Bernstein, T. Borger, M. Spinks, M. Donovan, V. Khudik, G. Shvets, T. Ditmire, and M. C. Downer, Quasi-monoenergetic laser-plasma acceleration of electrons to 2 GeV, Nat Commun **4,** 1988 (2013). https://doi.org/10.1038/ncomms2988
10. H. T. Kim, V. B. Pathak, K. Hong Pae, A. Lifschitz, F. Sylla, J. H. Shin, C. Hojbota, S. K. Lee, J. H. Sung, H. W. Lee, E. Guillaume, C. Thaury, K. Nakajima, J. Vieira, L. O. Silva, V. Malka, and C. H. Nam, Stable multi-GeV electron accelerator driven by waveform-controlled PW laser pulses, Sci Rep **7,** 10203 (2017). https://doi.org/10.1038/s41598-017-09267-1
11. A. Gonsalves, K. Nakamura, C. Lin, D. Panasenko, S. Shiraishi, T. Sokollik, C. Benedetti, C. B. Schroeder, C. G. R. Geddes, J. van Tilborg, J. Osterhoff, E. Esarey, C. Toth, and W. P. Leemans, Tunable laser plasma accelerator based on longitudinal density tailoring, Nature Phys **7,** 862–866 (2011). https://doi.org/10.1038/nphys2071
12. S. Steinke, J. van Tilborg, C. Benedetti, C. G. R. Geddes, C. B. Schroeder, J. Daniels, K. K. Swanson, A. J. Gonsalves, K. Nakamura, N. H. Matlis, B. H. Shaw, E. Esarey and W. P. Leemans, Multistage coupling of independent laser-plasma accelerators. Nature **530,** 190–193 (2016). https://doi.org/10.1038/nature16525
13. H. E. Martz, S. M. Glenn, J. A. Smith, C. J. Divin and S. G. Azevedo, Poly-Versus Mono-Energetic Dual-Spectrum Non-Intrusive Inspection of Cargo Containers, in IEEE Transactions on Nuclear Science, vol. 64, no. 7, pp. 1709-1718, July 2017. https://doi.org/ 10.1109/TNS.2017.2652455
14. S. Melton, C. Moss, R. Estep, Study of the Requirements for Monoenergetic Photon Sources, Los Alamos project report: DNDO Program manager, Namdoo Moon (2015).
15. J. Pruet, D. P. McNabb, C. A. Hagmann, F. V. Hartemann, and C. P. J. Barty, Detecting clandestine material with nuclear resonance fluorescence, Journal of Applied Physics 99, 123102 (2006). https://doi.org/10.1063/1.2202005
16. R. C. Runkle, D. L. Chichester, S. J. Thomson, Rattling nucleons: New developments in active interrogation of special nuclear material, Nucl. Inst. Meth. Phys. Res. A. 663 75-95 (2012). https://doi.org/10.1016/j.nima.2011.09.052
17. H. Schwoerer, B. Liesfeld, H.-P. Schlenvoigt, K.-U. Amthor, and R. Sauerbrey, Thomson-Backscattered X Rays From Laser-Accelerated Electrons, Phys. Rev. Letters, 96 (2006) 014802. https://doi.org/10.1103/PhysRevLett.96.014802
18. K. Ta Phuoc, S. Corde, C. Thaury, V. Malka, A. Tafzi, J. P. Goddet, R. C. Shah, S. Sebban, and A. Rousse, All-optical Compton gamma-ray source, Nature Photon **6,** 308–311 (2012). https://doi.org/10.1038/nphoton.2012.82

19. S. Chen, N. D. Powers, I. Ghebregziabher, C. M. Maharjan, C. Liu, G. Golovin, S. Banerjee, J. Zhang, N. Cunningham, A. Moorti, S. Clarke, S. Pozzi, D. P. Umstadter, MeV-Energy X Rays from Inverse Compton Scattering with Laser-Wakefield Accelerated Electrons, Phys. Rev. Lett. 110, (2013) 155003. https://doi.org/10.1103/PhysRevLett.110.155003
20. G. Sarri, D. J. Corvan, W. Schumaker, J. M. Cole, A. Di Piazza, H. Ahmed, C. Harvey, C. H. Keitel, K. Krushelnick, S. P. D. Mangles, Z. Najmudin, D. Symes, A. G. R. Thomas, M. Yeung, Z. Zhao, and M. Zepf, Ultra-high brilliance multi-MeV γ-ray beams from nonlinear relativistic Thomson scattering, Phys. Rev. Lett. 113 (2014) 224801. https://doi.org/10.1103/PhysRevLett.113.224801
21. The Future of Intense Ultrafast Lasers in the U.S., **Brightest Light Initiative** Workshop Report (OSA, Washington DC, March 2019). https://arxiv.org/abs/2002.09712.
22. S. M. Wiggins, R. P. Shanks, R. C. Issac, G. H. Welsh, M. P. Anania, E. Brunetti, G. Vieux, S. Cipiccia, B. Ersfeld, M. R. Islam, R. T. L. Burgess, G. Manahan, C. Aniculaesei, W. A. Gillespie, A. M. MacLeod, and D. A. Jaroszynski, High quality electron beams from a laser wakefield accelerator, CLEO/QELS: 2010 Laser Science to Photonic Applications, 2010, pp. 1-2.
23. C. Rechatin, J. Faure, A. Ben-Ismail, J. Lim, R. Fitour, A. Specka, H. Videau, A. Tafzi, F. Burgy, and V. Malka, Controlling the Phase-Space Volume of Injected Electrons in a Laser-Plasma Accelerator, Phys. Rev. Lett. 102, 164801 (2009). https://doi.org/10.1103/PhysRevLett.102.164801
24. S. G. Rykovanov, C. G. R. Geddes, J.-L. Vay, C. B. Schroeder, E. Esarey, W. P. Leemans, Quasi-monoenergetic femtosecond photon sources from Thomson Scattering using laser plasma accelerators and plasma channels, J. Phys B 47 234013 (2014). http://iopscience.iop.org/0953-4075/47/23/234013.
25. G. R. Plateau, C. G. R. Geddes, D. B. Thorn, M. Chen, C. Benedetti, E. Esarey, A. J. Gonsalves, N. H. Matlis, K. Nakamura, C. B. Schroeder, S. Shiraishi, T. Sokollik, J. van Tilborg, Cs. Toth, S. Trotsenko, T. S. Kim, M. Battaglia, Th. Stoehlker, and W. P. Leemans, Low-emittance electron bunches from a laser-plasma accelerator measured using single-shot X-ray spectroscopy, Phys. Rev. Lett. 109, 064802 (2012). https://doi.org/10.1103/PhysRevLett.109.064802
26. C. G. Durfee and H. Milchberg, Light pipe for high intensity laser pulses, Phys. Rev. Lett. 71 2409 (1993). https://doi.org/10.1103/PhysRevLett.71.2409
27. C. G. R. Geddes, C. Toth, J. van Tilborg, E. Esarey, C. Schroeder, J. Cary, and W. P. Leemans, Guiding of Relativistic Laser Pulses by Preformed Plasma Channels, Phys. Rev. Lett. 95 145002 (2005). https://doi.org/10.1103/PhysRevLett.95.145002.
28. E. Esarey, C. Schroeder, and W. P. Leemans, Physics of laser-driven plasma-based electron accelerators, Rev. Mod. Phys. 81 1229 (2009). https://doi.org/10.1103/RevModPhys.81.1229
29. C. Benedetti, C. B. Schroeder, E. Esarey, and W. P. Leemans, Quasi-matched propagation of ultra-short, intense laser pulses in plasma channels, Physics of Plasmas 19, 053101 (2012). https://doi.org/10.1063/1.4707393
30. C. G. R. Geddes, Cs. Toth, J. van Tilborg, E. Esarey, C. B. Schroeder, J. Cary , W. P. Leemans, Guiding of Relativistic Laser Pulses by Preformed Plasma Channels, Phys. Rev. Lett., V 95, no. 14, pp. 145002/1-4 (2005). https://doi.org/10.1103/PhysRevLett.95.145002

31. R. Lehe, M. Kirchen, I. A. Andriyash,B. B. Godfrey, J. L.Vay, A spectral, quasi-cylindrical and dispersion-free Particle-In-Cell algorithm, Comp. Phys. Comm., 203, 2016, pp 66-82. https://doi.org/10.1016/j.cpc.2016.02.007
32. https://github.com/fbpic/fbpic
33. A. Gonsalves, K. Nakamura, C. Lin, D. Panasenko, S. Shiraishi, T. Sokollik, C. Benedetti, C. B. Schroeder, C. G. R. Geddes, J. van Tilborg, J. Osterhoff, E. Esarey, C. Toth, and W. P. Leemans, Tunable laser plasma accelerator based on longitudinal density tailoring, Nature Phys **7,** 862–866 (2011). https://doi.org/10.1038/nphys2071
34. H.-E. Tsai, K. K. Swanson, S. K. Barber, R. Lehe , D. E. Mittelberger, S. Steinke, K. Nakamura, J. van Tilborg, C. Schroeder, E. Esarey, C. G. R. Geddes, and W. P. Leemans, Control of quasi-monoenergetic electron beams from laser-plasma accelerators with adjustable shock density profile, Physics of Plasmas 25, 043107 (2018). https://doi.org/10.1063/1.5023694
35. T. C. Chiou and T. Katsouleas, C. Decker and W. B. Mori, J. S. Wurtele and G. Shvets, J. J. Su, Laser wake-field acceleration and optical guiding in a hollow plasma channel, Physics of Plasmas 2, 310 (1995). https://doi.org/10.1063/1.871107
36. A. Bonatto, C. B. Schroeder, J.-L. Vay, C. G. R. Geddes, C. Benedetti, E. Esarey, and W. P. Leemans, Passive and active plasma deceleration for the compact disposal of electron beams, Physics of Plasmas 22, 083106 (2015). https://doi.org/10.1063/1.4928379
37. L.-L. Yu, E. Esarey, C. B. Schroeder, J.-L. Vay, C. Benedetti, C. G. R. Geddes, M. Chen, and W. P. Leemans, Two-Color Laser-Ionization Injection, Phys. Rev. Lett. 112, 125001 (2014). https://doi.org/10.1103/PhysRevLett.112.125001
38. E. Esarey, J. Krall, and P. Sprangle, Envelope analysis of intense laser pulse self-modulation in plasmas, Phys. Rev. Lett. **72**, 2887 (1994). https://doi.org/10.1103/PhysRevLett.72.2887
39. E. Esarey, J. Krall, and P. Sprangle, Hose-Modulation Instability of Laser Pulses in Plasmas, Phys. Rev. Lett. **73**, 3544 (1994). https://doi.org/10.1103/PhysRevLett.73.3544
40. C. Benedetti, C. B. Schroeder, E. Esarey, F. Rossi, and W. P. Leemans, Numerical investigation of electron self-injection in the nonlinear bubble regime, Physics of Plasmas 20, 103108 (2013). https://doi.org/10.1063/1.482481
41. M. Kirchen, S. Jalas, P. Messner, P. Winkler, T. Eichner, L. Hübner, T. Hülsenbusch, L. Jeppe, T. Parikh, M. Schnepp, and A. R. Maier, Optimal Beam Loading in a Laser-Plasma Accelerator, Phys. Rev. Lett. 126, 174801 (2021). https://doi.org/10.1103/PhysRevLett.126.174801
42. R. Lehe, C. Thaury, E. Guillaume, A. Lifschitz, and V. Malka, Laser-plasma lens for laser-wakefield accelerators, Phys. Rev. ST Accel. Beams 17, 121301 (2014). https://doi.org/10.1103/PhysRevSTAB.17.121301
43. J.-L. Vay, Noninvariance of Space- and Time-Scale Ranges under a Lorentz Transformation and the Implications for the Study of Relativistic Interactions, Phys. Rev. Lett. 98, 130405 (2007). https://doi.org/10.1103/PhysRevLett.98.130405
44. K. Khrennikov, J. Wenz, A. Buck, J. Xu, M. Heigoldt, L. Veisz, and S. Karsch, Tunable All-Optical Quasimonochromatic Thomson X-Ray Source in the Nonlinear Regime, Phys. Rev. Lett. 114, 195003 (2015). https://doi.org/10.1103/PhysRevLett.114.195003
45. H.-E. Tsai, X. Wang, J. M. Shaw, Z. Li, A. V. Arefiev, X. Zhang, R. Zgadzaj, W. Henderson, V. Khudik, G. Shvets, and M. C. Downer , Compact tunable Compton x-ray

source from laser-plasma accelerator and plasma mirror, Physics of Plasmas 22, 023106 (2015). https://doi.org/10.1063/1.4907655
46. G. Golovin, S. Banerjee, C. Liu, S. Chen, J. Zhang, B. Zhao, P. Zhang, M. Veale, M. Wilson, P. Seller, and D. Umstadter, Intrinsic beam emittance of laser-accelerated electrons measured by x-ray spectroscopic imaging, Sci Rep 6, 24622 (2016). https://doi.org/10.1038/srep24622
47. F. He, Y. Y. Lau, D. P. Umstadter, and R. Kowalczyk, Backscattering of an Intense Laser Beam by an Electron, Phys. Rev. Lett. 90, 055002 (2003). https://doi.org/10.1103/PhysRevLett.90.055002